Supplementary Information

Charge-compensated co-doping stabilizes robust hafnium oxide ferroelectricity

Gang Li,[1,2] Yulin Liu,[3] Shaoan Yan,[2] Ningjie Ma,[3] Yongguang Xiao,[3] Minghua Tang,[3,*] Zhilin Long[1,*]

[1]College of Civil Engineering, Xiangtan University, Xiangtan 411105, China

[2]School of Mechanical Engineering and Mechanics, Xiangtan University, Xiangtan 411105, China

[3]School of Materials Science and Engineering, Xiangtan University, Xiangtan 411105, China

Email: tangminghua@xtu.edu.cn, longzl@xtu.edu.cn

1. Crystal structure modelling and dopant atom characterization

Tab. S1 Lattice parameters (in Å) of the bulk phases of HfO_2 compared with previous theory computational studies and experiment. For the monoclinic (m) phase, α is the angle between **a** and **c**, which is the only non-perpendicular angle for this phase.

Phase	Lattice parameters	Our work	Theory [1]	Experiment
$P4_2/nmc$ (t)	a, c (Å)	5.03, 5.13	5.07, 5.19	5.06, 5.20 [2]
$P2_1/c$ (m)	a, b, c (Å)	5.08, 5.16, 5.18	5.11, 5.18, 5.30	5.07, 5.14, 5.29
	α	99.7°	99.6°	99.7° [3]
$Pca2_1$ (f)	a, b, c (Å)	5.21, 5.00, 5.03	5.25, 5.04, 5.07	5.24, 5.06, 5.07 [4]

Tab. S2 Impact of dopant on the phase stability of HfO_2, "↓" and "↑" mean the phase energy difference $\Delta E^{\text{f-m}}/\Delta E^{\text{t-m}}$ lower and rise when dopant concentration increases, respectively. "-" means no data available. The subscripts "min" and "max" of the arrows indicate smaller and larger changes, respectively. The dopant concentration falls in the range of 0%–12.5%.

Valence	Dopant	Phase (This work)		Phase (Other)	
		f	t	f	t
2	Mg	$\downarrow_{\text{max}}$	$\downarrow_{\text{min}}$	$\downarrow_{\text{max}}$[5]	$\downarrow_{\text{min}}$[5]
	Ca	$\downarrow_{\text{max}}$	$\downarrow_{\text{min}}$	$\downarrow_{\text{max}}$[5]	$\downarrow_{\text{min}}$[5]
	Sr	$\downarrow_{\text{max}}$	$\downarrow_{\text{min}}$	$\downarrow_{\text{max}}$[5]	$\downarrow_{\text{min}}$[5]
3	Al	$\downarrow_{\text{min}}$	$\downarrow_{\text{max}}$	$\downarrow_{\text{min}}$[6]	$\downarrow_{\text{max}}$[6]
	Y	$\downarrow_{\text{max}}$	$\downarrow_{\text{min}}$	$\downarrow_{\text{max}}$[6]	$\downarrow_{\text{max}}$[6]
	La	$\downarrow_{\text{max}}$	$\downarrow_{\text{min}}$	$\downarrow_{\text{max}}$[6]	$\downarrow_{\text{min}}$[6]
	Gd	$\downarrow_{\text{max}}$	$\downarrow_{\text{min}}$	$\downarrow_{\text{max}}$[7]	$\downarrow_{\text{min}}$[7]
4	Si	$\downarrow_{\text{min}}$	$\downarrow_{\text{max}}$	$\downarrow_{\text{min}}$[8]	$\downarrow_{\text{max}}$[8]
	Ti	$\uparrow_{\text{min}}$	$\downarrow_{\text{max}}$	$\uparrow_{\text{min}}$[8]	$\downarrow_{\text{max}}$[8]
	Zr	$\downarrow_{\text{min}}$	$\downarrow_{\text{min}}$	$\downarrow_{\text{min}}$[8]	$\downarrow_{\text{min}}$[8]
	Sn	$\downarrow_{\text{min}}$	$\downarrow_{\text{max}}$	$\downarrow_{\text{min}}$[8]	$\downarrow_{\text{max}}$[8]
	Pb	$\downarrow_{\text{max}}$	$\downarrow_{\text{max}}$	-	-
5	V	$\downarrow_{\text{min}}$	$\downarrow_{\text{max}}$	$\downarrow_{\text{min}}$[7]	$\downarrow_{\text{max}}$[7]
	Nb	$\uparrow_{\text{max}}$	$\uparrow_{\text{max}}$	$\uparrow_{\text{max}}$[7]	$\uparrow_{\text{max}}$[7]
	Ta	$\uparrow_{\text{max}}$	$\uparrow_{\text{max}}$	$\uparrow_{\text{max}}$[7]	$\uparrow_{\text{max}}$[7]

Tab. S3 Ionic radius and electronegativity of dopants.

|	D^{4+}	D^{2+}			D^{3+}				D^{4+}					D^{5+}		
	Hf	Mg	Ca	Sr	Al	Y	La	Gd	Si	Ti	Zr	Sn	Pb	V	Nb	Ta
Ionic radius (Å)	0.71	0.72	1.00	1.18	0.53	0.90	1.03	0.94	0.40	0.61	0.72	0.69	0.78	0.54	0.64	0.64
Electronegativity	1.31	1.31	1.00	0.95	1.60	1.22	1.10	1.20	1.90	1.54	1.33	1.96	1.87	1.63	1.60	1.50
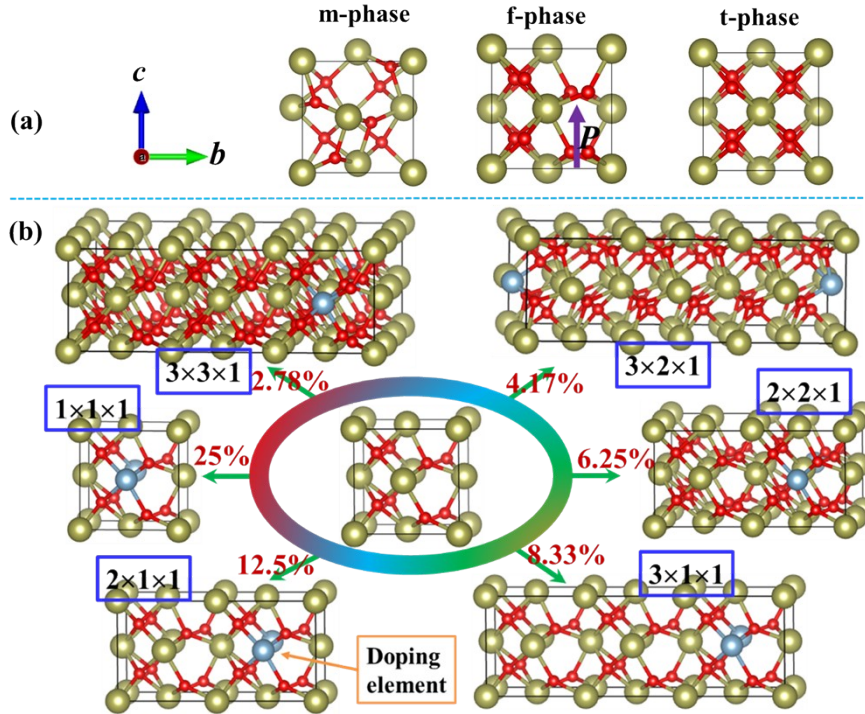
Fig. S1 (a) Crystal structure of three phases, (b) Different supercell structures constructed based on the f-phase HfO$_2$, and doped HfO$_2$ model by doping a dopant in these supercell. This modeling also applies to doped m-phase and doped t-phase.

## 2. Ferroelectric f-phase fraction and magnitude of spontaneous polarization
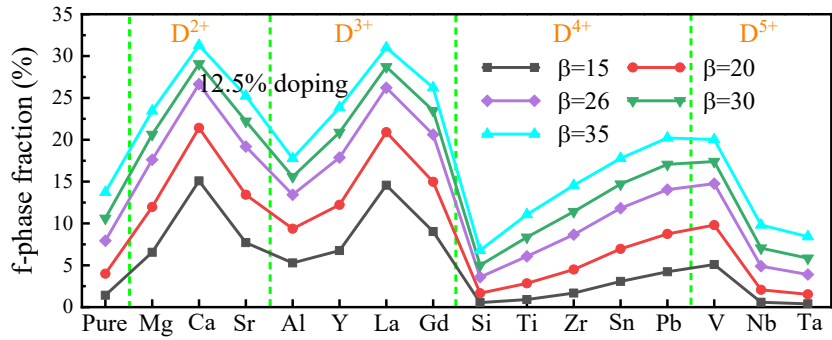
Fig. S2 The f-phase fractions of HfO$_2$ polymorphs in the presence of different dopants under different β values. The valence states of different dopants are separated by green dotted lines.
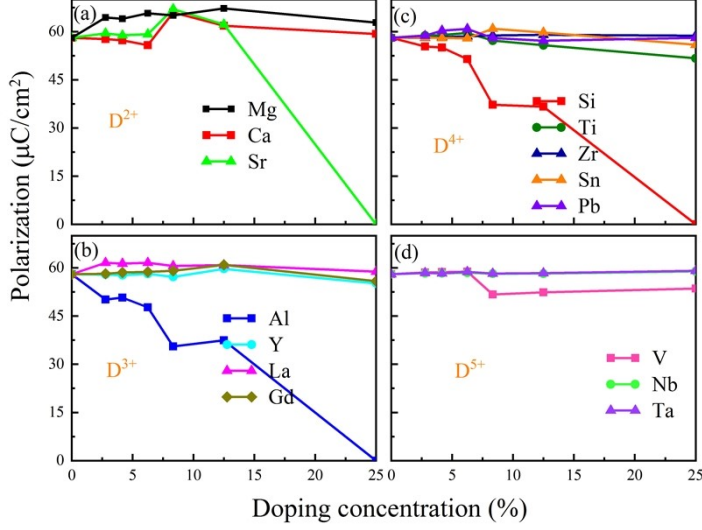
Fig. S3 Polarization magnitude of doped HfO_2 with (a) D^{2+}, (b) D^{3+}, (c) D^{4+}, and (d) D^{5+} elements under different doping concentrations. Once it is difficult to clearly identify the ferroelectric phase morphology during relaxation at higher doping concentrations, we set its polarization magnitude to zero.

3. Total phase energy and phase structure transformation under carrier conditions
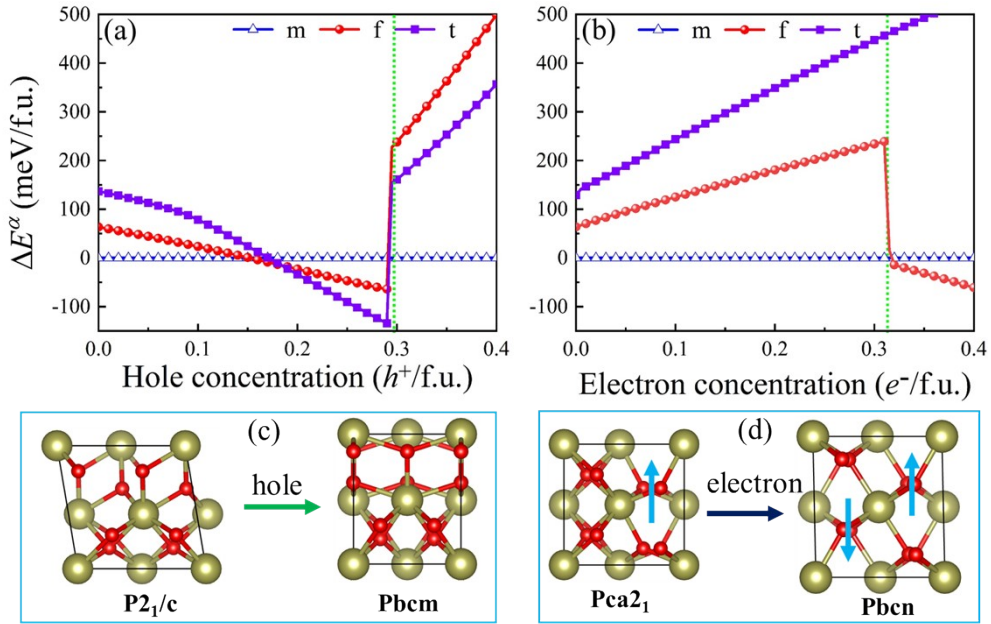
Fig. S4 Phase energy difference ΔE of HfO_2 as a function of hole (a) and electron (b) concentration. The vertical green dashed line indicates that the phase transition occurs at this doping concentration. Phase transition diagram under (c) hole doping and (d) electron doping.

The cyan arrow in the (d) indicates the polarization direction.

Tab. S4 Phase energy difference ΔE between Pca2$_1$ (Pbcn) phase and P2$_1$/c phase under different Ta doping concentrations.

	Ta concentration = 25%		Ta concentration = 50%	
	Pca2$_1$	Pbcn	Pca2$_1$	Pbcn
$\Delta E^{\alpha\text{-m}}$ (meV/f.u.)	104.23	71.27	113.33	-13.39

## 4. DOS and 3D charge density distribution of phase with different dopants
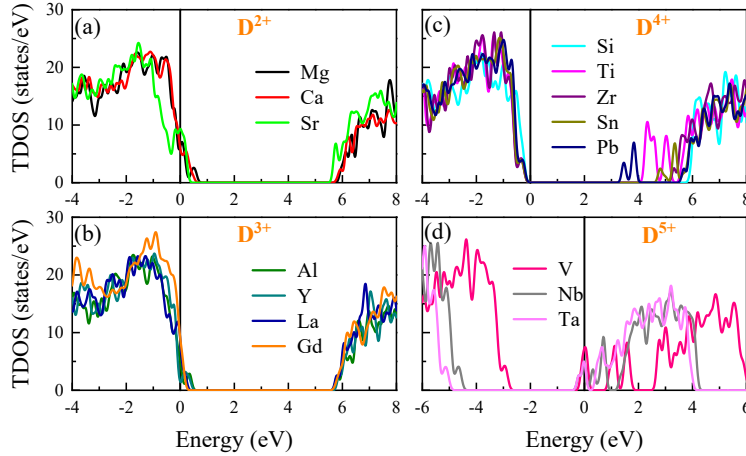
Fig. S5 The total density of state (TDOS) of the (a) D^{2+}, (b) D^{3+}, (c) D^{4+}, (d) D^{5+} elements doped m-phase HfO$_2$ with doping concentration of 12.5% using HSE06 hybrid functional. The zero of energy represents the Fermi level in this and subsequent DOS.
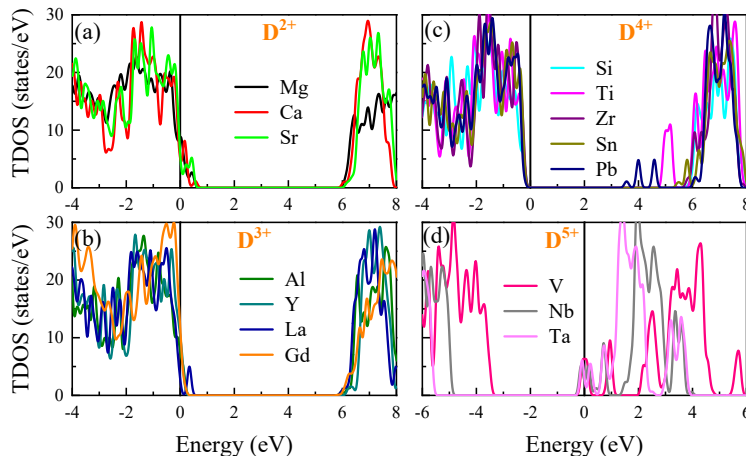
Fig. S6 The TDOS of the (a) D^{2+}, (b) D^{3+}, (c) D^{4+}, and (d) D^{5+} element doped t-phase HfO$_2$ with doping concentration of 12.5% using HSE06 hybrid functional.
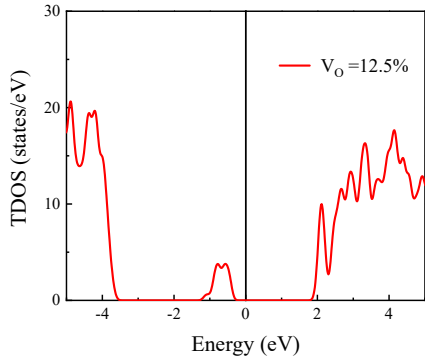
Fig. S7 The TDOS of the f-phase HfO$_2$ with oxygen vacancies concentration of 12.5% using HSE06 hybrid functional.
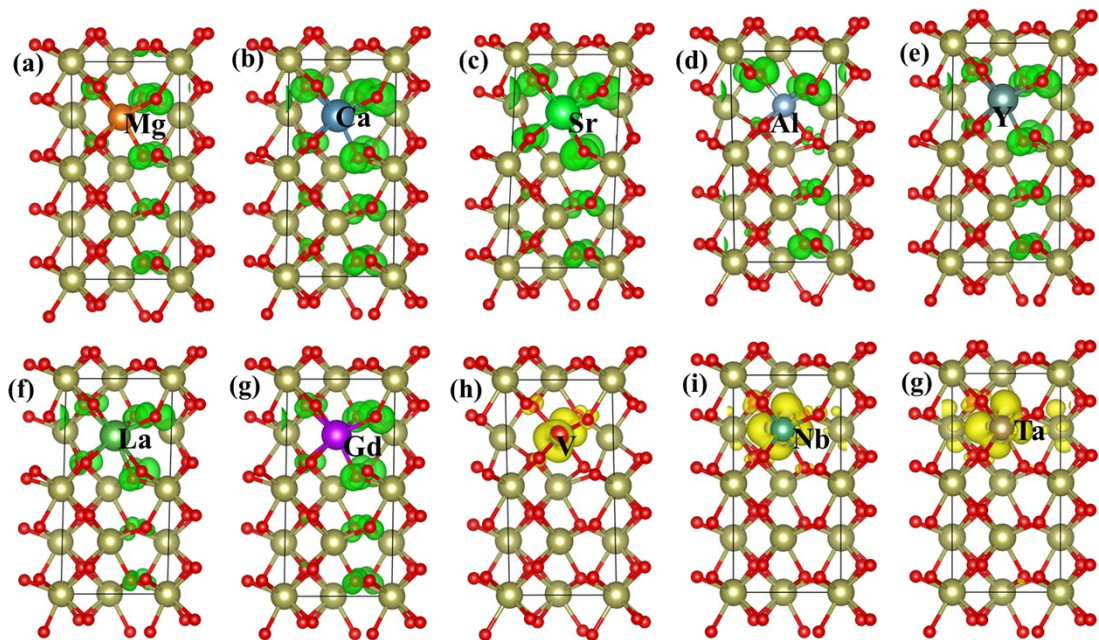

Fig. S8 The 3D charge density projected on bands forming the metallic states in the doped f-phase HfO$_2$ with doping concentration of 12.5%. (a) Ca, (b) Sr, (c) Ba, (d) Al, (e) Y, (f) La, (g) Gd, (h) V, (i) Nb, (g) Ta. The energy range of 3D charge density in the V, Nb, and Ta-doped HfO$_2$ is [-1, 0], while the energy range of other doped HfO$_2$ is [0, 1]. Therefore, the holes and electrons are depicted by green and yellow isosurfaces, respectively.
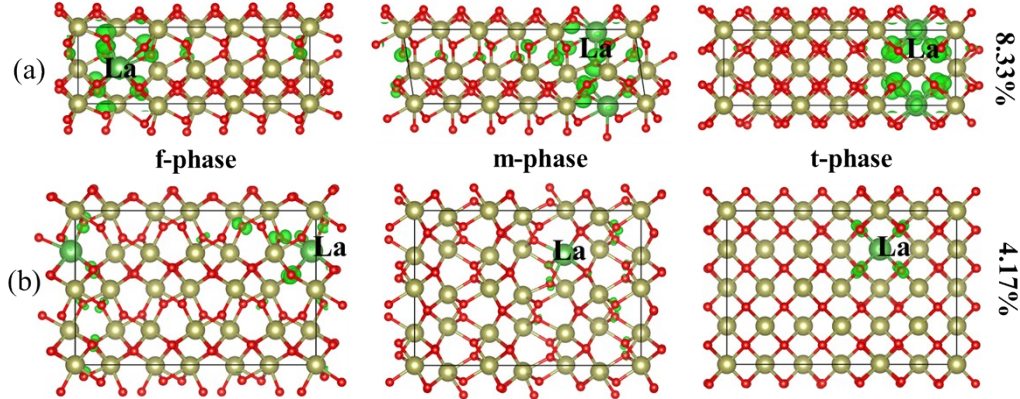
Fig. S9 The 3D charge density distribution of La-doped HfO$_2$ in different phases with a doping concentration of (a) 8.33% and (b) 4.17%.

5. Phase stability and phase fraction of Ca@2V, Ca@V$_O$, and La@V$_O$ systems
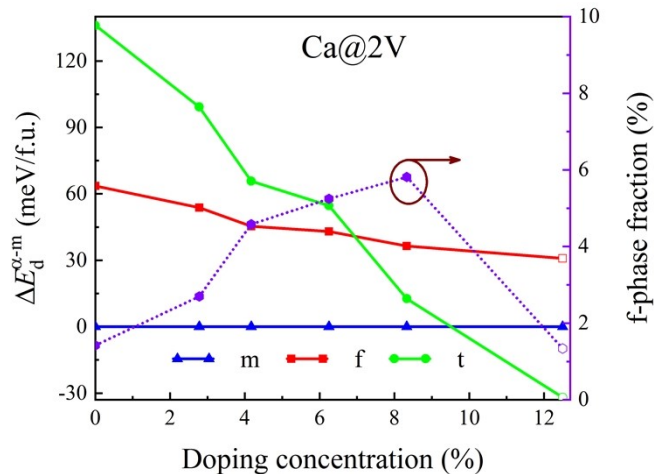

Fig. S10 Phase energy difference ΔE_d of Ca@2V co-doped HfO$_2$ and the f-phase fraction as a function of doping concentration. To achieve electrical neutrality within the system, two V atoms are needed for each Ca atom. Although the phases mostly retained their structural characteristics (solid symbols) upon doping, at higher doping concentrations, it is difficult to clearly identify the doping phase structure after relaxation, which is indicated by open symbols.
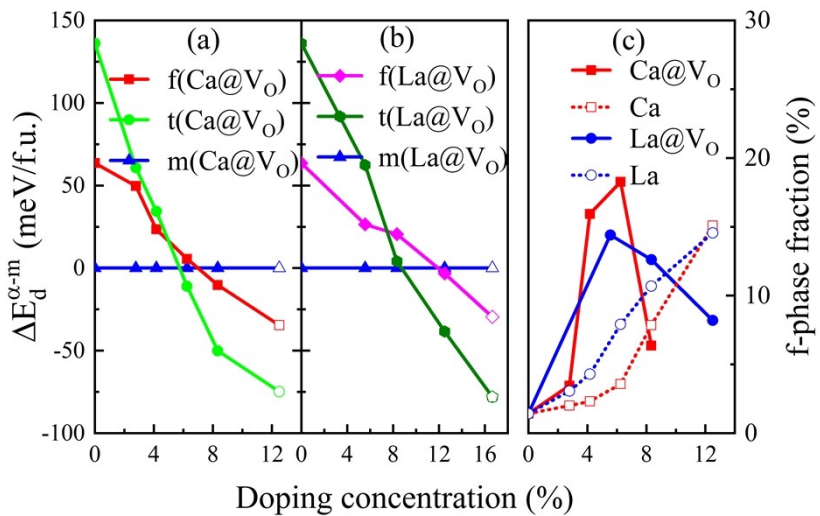
Fig. S11 Phase total energy difference ΔE_d of (a) Ca@V_O and (b) La@V_O co-doped HfO$_2$ and their f-phase fraction (c) as a function of doping concentration. In which the f-phase fraction of single element Ca and La-doped HfO$_2$ are used for comparison. Although the phases mostly retained their structural characteristics (solid symbols) upon doping in (a) and (b), at higher doping concentrations, it is difficult to clearly identify the doping phase structure after relaxation, which is indicated by open symbols.

References

1 M. Dogan, N. Gong, T. P. Ma and S. Ismail-Beigi, *Phys. Chem. Chem. Phys.*, 2019, **21**, 12150.

2 I. MacLaren, T. Ras, M. MacKenzie, A. J. Craven, D. W. McComb and S. De Gendt, *J. Electrochem. Soc.*, 2009, **156**, G103.

3 R. Ruh and P. W. R. Corfield, *J. Am. Ceram. Soc.*, 1970, **53**, 126.

4 E. D. Grimley, T. Schenk, T. Mikolajick and J. M. LeBeau. *Adv. Mater. Interfaces*, 2018, **5**, 1701258.

5. R. Materlik, Technische Universität Dresden, 2019.

6 R. Materlik, C. Kunneth, M. Falkowski, T. Mikolajick, and Alfred Kersch, *J. Appl. Phys.*, 2018, **123**, 164101.

7 R. Batra, T. D. Huan, G. A. Rossetti, Jr., and R. Ramprasad, *Chem. Mater.*, 2017, **29**, 9102.

8 C. Künneth, R. Materlik, M. Falkowski, and A. Kersch, *ACS Appl. Nano Mater.*, 2018, **1**, 254.